Wear 538-539 (2024) 205232

Contents lists available at ScienceDirect

Wear

journal homepage: www.elsevier.com/locate/wear

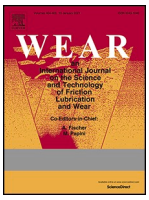

Modelling the adhesion enhancement induced by sand particle breakage at the wheel-rail interface

Bin Zhang [a], Sadegh Nadimi [a,*], Roger Lewis [b]

[a] School of Engineering, Newcastle University, Newcastle upon Tyne, NE1 7RU, United Kingdom
[b] Leonardo Centre for Tribology, Department of Mechanical Engineering, University of Sheffield, Sheffield, S13JD, United Kingdom

ARTICLE INFO

Keywords:
Wheel-rail adhesion
Particle breakage
Particle size
Friction

ABSTRACT

The adhesion at the wheel-rail contact is critical in train operation. Low adhesion leads to a longer distance for a train to accelerate and brake, and this may cause serious accidents. Sand particles are applied onboard trains at the wheel-rail contact to enhance the adhesion level. In this study, a finite element model is developed to investigate the mechanical behaviour of sand particles in a wheel-rail contact and how they affect the adhesion level. The acceleration and braking events using rolling/slipping and sliding contacts are simulated. Morphological properties of sand particles such as size and aspect ratio are considered. The adhesion enhancement is quantified from each simulation for comparison. The results indicate that the adhesion enhancement during the first contact between the wheel and sand particles is negligible and starts to increase when the wheel is rolling on the fragments. Its magnitude is controlled by the new third-body layers generated during the particle breakage under both rolling and sliding contacts. However, under sliding contact, when a similar amount of fragments is considered, the coarser particles with a larger aspect ratio tend to produce a higher adhesion enhancement.

1. Introduction

Adhesion[1] in the wheel-rail contact significantly influences the efficiency of traction and braking operations [1]. During traction operation, it takes a longer time for trains to achieve the required speed through acceleration when low adhesion exists. It leads to delays and general disruption which is one of the greatest costs to the industry [2]. While in braking operation, the lack of adhesion increases the braking distance and could cause SPADs (signals passed at danger) or collisions in the worst-case scenario [3]. These phenomena could occur when adhesion values are lower than 0.2 for traction and 0.09 for braking operations respectively [2]. The presence of poor adhesion is mainly due to contamination on the rail head, such as leaves during autumn [4], water from the atmosphere [5], oils from lineside work [6] and iron oxides [7]. Sanding is a widely adopted adhesion recovery method in most railway networks since the early days of operation. When low adhesion presents, sand particles are fired at the wheel-rail interface from an on-board device to break down contamination and enhance the adhesion level. It usually occurs automatically during emergency braking, but is a manual process for the control of traction.

During the past few decades, research has been carried out to investigate the consequences after sand particles entrained the wheel-rail contact. Experiments have been established across a range of scales (e.g., twin-disc set-up, linear full-scale rig and field tests) to investigate the adhesion restoration and leaf layer removal induced by sand particles, as well as the traction enhancers [1]. In order to optimise the railway sanding system, sand entrainment has been investigated for different hose types, hose positions and crosswinds using an experimental approach [8]. Furthermore, numerical simulations have been conducted to investigate the sander efficiency affected by the coefficient of restitution, coefficient of friction, particle size, particle shape and crosswinds [9]. Recently, alternative materials have been tested and compared for the purpose of replacing the original sand [10]. All these studies explain the advantages and limitations of sanding application in railway operation well.

When it comes to the morphological effect of sand particles, the size distribution and shape features are specifically described in the Rail Safety and Standards Board (RSSB) standard GMRT2461 for traction and braking operations [11]. According to operational experience, fine-particle sand is better for acceleration, while coarse-particle sand is better for braking [11]. Additionally, particle size is proportional to the degree of adhesion increase [12,13]. Fine and medium-sized sand

* Corresponding author.
E-mail address: sadegh.nadimi-shahraki@newcastle.ac.uk (S. Nadimi).

[1] In the railway industry "adhesion" or "adhesion coefficient" is defined as the amount of traction present when the wheel-rail contact enters partial slip.

https://doi.org/10.1016/j.wear.2023.205232
Received 3 February 2023; Received in revised form 9 November 2023; Accepted 27 December 2023
Available online 28 December 2023

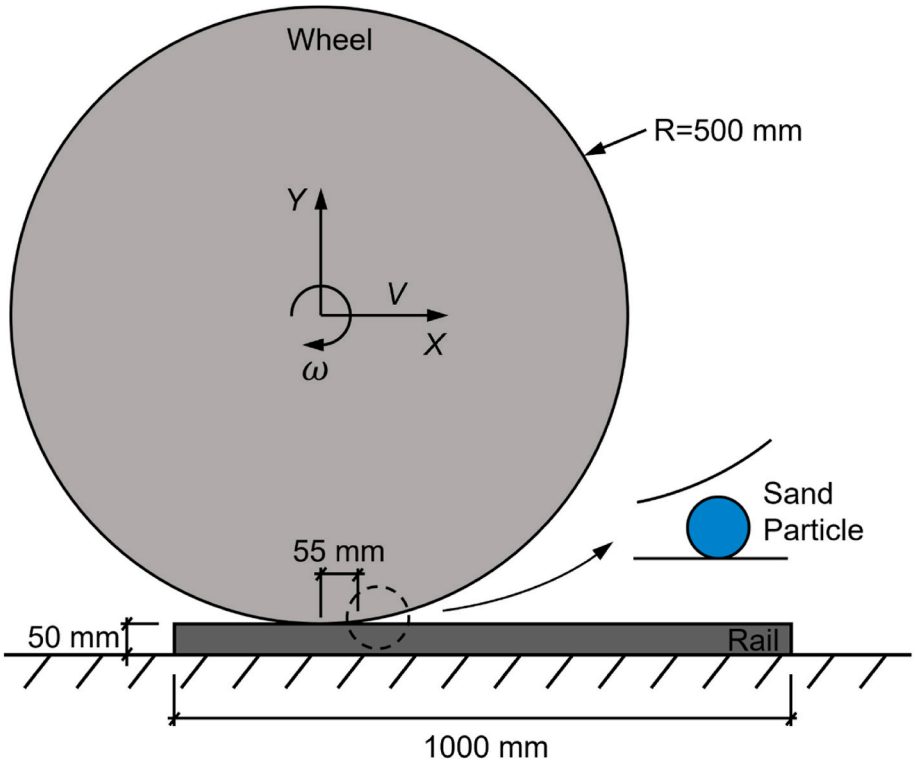

Fig. 1. Schematic diagram of the Finite Element model.

particles (0.06–0.3 mm and 0.3–0.6 mm, respectively) are more likely to result in isolation (good electrical contact between wheel and rail is essential for train detection in signal systems), according to research on the relationship between particle size and risk of isolation [14]. They suggested that this might be due to smaller particles not breaking up and being ejected upon entering the contact, thus allowing a layer of sand to build up. The particle-size effects based on standard sand and its micro-fragments were examined by Shi et al. using a twin-disc set-up [15]. They discovered that the micro-fragments enhance adhesion at a smaller cost of wheel-rail wear and damage. Skipper et al. [16] performed particle characterization followed by high pressure torsion (HPT) testing. Based on the outcomes, a less circular particle is preferable for low adhesion conditions, and an optimum particle size exists when mitigating against leaf layers.

While it is clear that initial particle size and how the particles entrain and break up at the wheel-rail interface are influential on adhesion enhancement as well as possible damage to the wheel and rail, there is little research regarding the exact physical mechanisms of the sand particles fracture process and how fragments behave at the wheel-rail interface. In this study, the finite element method (FEM) coupled with cohesive interface elements (CIEs) is used to study the influence of sand particle breakage on adhesion enhancement in wheel-rail contact. A wheel-rail model is developed with boundary conditions assigned to reproduce actual traction and braking operations. Particle morphology such as particle size and shape are analysed to observe their influences on adhesion enhancement at the wheel-rail interface before and after the particle breakage. Finally, the adhesion enhancements from different simulations are compared. This study provides new insights into the fracture behaviours of sand particles and their fragmentation effect on adhesion enhancement. The method used in this study will provide a procedural framework for other railway sanding studies.

Table 1
Summary of the FEM model.

	Wheel	Rail	Sand particles
Part Type	Discrete rigid	Deformable	Deformable (CIEs added)
Geometry	Circle	Rectangle	Circle/Ellipse
Boundary conditions	Horizontal displacement Concentrated force Traction operation (0.242 radians) Braking operation (0 radians)	Encastre	Free

2. Method and material

The 2D numerical simulation starts with the sand particles entering the wheel-rail contact. When the stress coming from the wheel-rail contact achieves the maximum strength of the sand particles, crack initiation and propagation occur, followed by particle fragmentation. The FEM is used to simulate the continuous event where the particle is interacting with the wheel and the rail, and the CIEs are used to trigger the discontinuous event when the particle breaks into fragments. The Abaqus/Explicit is adopted due to its efficiency in solving discontinuous problems.

2.1. Numerical model

To reproduce the wheel-rail contact, a finite element model is generated in Abaqus, as illustrated in Fig. 1, where the inset shows a zoomed view of the sand particle. The included three parts are: (a) the wheel is defined as a rigid body to avoid complex elastic deformations due to multiple motions, which are not trivial to compute numerically. It is assigned with a displacement in the X direction (ca. 110 mm, which is an adequate length for the wheel to break particles in element size fragments and pass them entirely) and with a 60 kN concentrated force at the centre, which is a typical load for a passenger train [10]. For traction operation, the wheel is subjected to an angle of rotation equal to 0.242 radians to simulate the 10 % slip used in experiments [17]. For braking operation, no rotation is provided to the wheel in order to

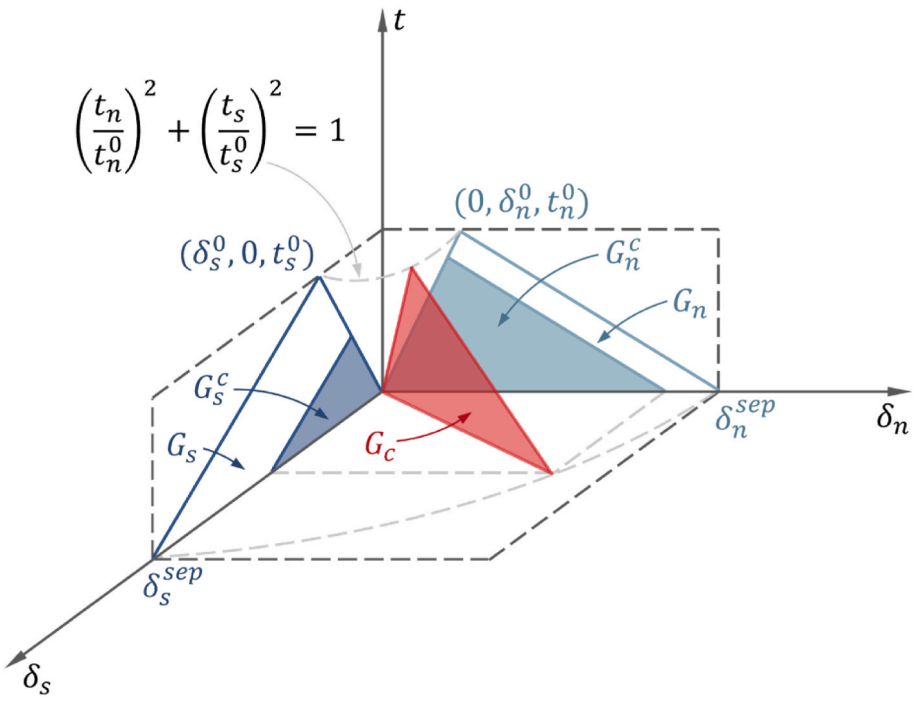

Fig. 2. Bi-linear cohesive traction-separation law, the quadratic nominal stress criterion and the mixed-mode fracture criterion.

simulate pure sliding, which is an extreme case of this operation; (b) the rail is a deformable body to allow the sand particle and fragments entry the wheel-rail contact easily. It has a fixed boundary condition at the bottom to limit the motion of the rail from all directions. From some preliminary simulation results, the stress distribution and associated deformations only occur within the rail sub-surface area, therefore the rail depth has been reduced from actual size to 50 mm to expedite the simulation; (c) the sand particles are deformable bodies as well, but have been modelled with CIEs to simulate the fracture behaviour. Table 1 summarizes the information of the mentioned parts and their boundary conditions.

During the simulation, the 60 kN concentrated force is considered the normal force. The tangential force along the moving direction is recorded throughout the entire simulation. The overall traction can be quantified using the equation below:

$$\mu = \frac{F}{N} \tag{1}$$

Table 2
FEM Material parameters used in this study.

	Parameter	Value
Solid Elements (Particle)		
Density	$\rho\ (kg/m^3)$	2500
Young's Modulus	$E\ (GPa)$	63
Poisson's ratio	ϑ	0.22
Solid Elements (Rail)		
Density	$\rho\ (kg/m^3)$	7800
Young's Modulus	$E\ (GPa)$	210
Poisson's ratio	ϑ	0.30
Cohesive interface elements (CIEs)		
Normal stiffness	$k_n\ (N/mm^2)$	63,000
First shear stiffness	$k_s\ (N/mm^2)$	31,500
Tensile strength	$N_{max}\ (MPa)$	25
First shear strength	$S_{max}\ (MPa)$	12
Mode I fracture energy	$G_n\ (N/mm)$	0.1
Mode II fracture energy	$G_s\ (N/mm)$	0.2
Material parameter	η	2
Contact law		
Particle-to-Structure friction coefficient	μ	0.5

where μ is the adhesion coefficient, F is the tangential force and N is the normal force.

In addition to the wheel-rail contact is assumed to be frictionless, the coefficient of friction between fragment-to-wheel and fragment-to-rail, and fragment-to-fragment are set to 0.5, which is the value for dry contact observed from experiments [15] and applied in numerical simulations [18]. As a result, the calculated μ from this model is only considering the traction force came from these micro frictional contacts and interlocking of the fragments. To separate this value from the common adhesion coefficient μ, an adhesion enhancement is used in this study to represent the calculated results.

2.2. Material properties

All meshes are generated using 3-node linear plane strain triangle (CPE3) elements. Each CPE3 can locally deform depending on the current nodal forces. For sand particles, cohesive elements (COH2D4) are placed at the interface of CPE3 elements [19]. Since the CIE is zero-thickness, the geometry of the mesh has not been changed, but every element is now bonded by the CIEs. When the normal stress or shear stress at the CIE reaches a threshold value, the CIE starts to vanish thus debonding between elements occurs. This behaviour of the CIE can be illustrated by the bi-linear cohesive traction-separation law, and the quadratic nominal stress criterion is used to initiate the crack propagation:

$$\left(\frac{t_n}{t_n^0}\right)^2+\left(\frac{t_s}{t_s^0}\right)^2=1 \tag{2}$$

where t_n and t_s donate the nominal stresses in normal and first shear direction, respectively. t_n^0 and t_s^0 donate the maximum allowable nominal stresses in normal and first shear direction, respectively.

Another significant parameter to be considered for utilizing the CIE is fracture energy. It is used as a definition to specify the damage evolution and quantify the energy dissipated due to fracture. Due to the nature of 2D FE modelling, only two modes of fracture energy have been involved, thus the normal mode (mode I) and the first direction shear mode (mode II). Since the mix mode (mode I + mode II) fractures are the dominant

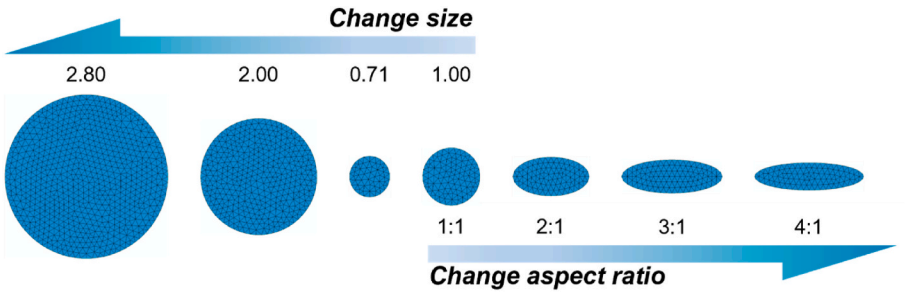

Fig. 3. Particles mesh in different sizes and shapes.

Table 3
Mesh composition of sand particles.

	Mesh dimension (mm)	Element size (mm)	CPE3 elements
Size	0.71	0.10	92
	1.00	0.10	179
	2.00	0.10	733
	2.80	0.10	1388
Shape	1:1 (1.00/1.00)	0.10	179
	2:1 (1.36/0.68)	0.10	170
	3:1 (1.80/0.60)	0.10	186
	4:1 (2.00/0.50)	0.10	174

failure behaviours of brittle materials compared to single mode fractures, the Benzeggagh-Kenane (B–K) fracture criterion [20] is utilized to define the mixed-mode fracture energy:

$$G^c = G_n^c + \left(G_s^c - G_n^c\right)\left\{\frac{G_s}{G_n + G_s}\right\}^{\eta} \tag{3}$$

where G^c represents the mixed-mode fracture energy. G_n^c and G_s^c represent the mode I and mode II fracture energies respectively. η is a semi-empirical criterion exponent applied to delamination initiation and growth. Since there are limited studies on η of geomaterials, the parameter values of resin ranging from 2 (brittle) to 3 (ductile) are used in this study [21]. Fig. 2 summarizes the bi-linear cohesive traction-separation law, the quadratic nominal stress criterion and the mixed-mode fracture criterion.

Material parameters of quartz sand are selected to investigate the fracture behaviour. Table 2 summarizes the material parameters used in this study, including density (ρ), elastic modulus (E), Poisson's ratio (ϑ), tensile strength (N_{max}) and shear strength (S_{max} and T_{max}) and CIE stiffness' (k_n and k_s), fracture energy (G_n, and G_S) and material parameter (η). These parameters are referenced from a previous study [22].

2.3. Mesh forms

The variation of sand morphology (size and shape) alters their mechanical properties, such as the ultimate strength, friction, fracture behaviour, fragment distribution, etc., which could influence the adhesion level at the wheel-rail interface. In this study, it is assumed that all sand particles are regular shapes (i.e., circle and ellipse). Circular meshes are generated to investigate the size effect and ellipsoidal meshes are created to explore the shape effect. The diameters of circular meshes are varying from 0.71 mm to 2.80 mm according to the RSSB standard GMRT2461 [10,11]. The aspect ratios of ellipsoidal meshes are increasing from 1:1 to 4:1. The generated sand particle meshes in different sizes and aspect ratios are illustrated in Fig. 3.

Considering the average fragment size of 100 μm observed from experiments [10], a constant element size of 100 μm is assigned to all particle meshes. This element size has a good representation of the real fragmentation process of sand particles at the wheel-rail interface, as it allows all particle meshes to break into element-size fragments during the simulation. Additionally, based on the mesh sensitivity study from the previous research [22], the element size to mesh size ratio used in this study is in the acceptable range. The composition of all the sand particle meshes used in this study is listed in Table 3.

3. Result and discussion

This section focuses on statistical analysis and results discussion linking the impact of particle size and shape to the adhesion enhancement triggered by sand particle fragmentation at the wheel-rail contact.

3.1. Particle fracture behaviour

Due to the nature of rigid/deformable body in Abaqus, the rail is indented by the particles at the wheel-rail contact that causes the variation of adhesion force, while the wheel is undeformed. According to the particle state during the simulation, the whole simulation process can be classified into three stages, as shown in Fig. 4: (1) prior-to-fracture stage; (2) the fracture stage, where the first contact between the wheel and particle is happening, followed by multiple contacts with particle fragments. The first contact (Fig. 4(a) and (d)) of each particle occurs slightly differently due to the size difference, as all particles are located 55 mm away from the wheel. For traction operation, the fragments are intended to remain at the original position or move towards the wheel-rail contact, as shown in Fig. 4(b). On the contrary, during the braking operation, fragments have been spread further away from their original place as a consequence of the chopping force induced by the sliding wheel, as illustrated in Fig. 4(e); 3) post-fracture stage, where the particle is fully fractured and the wheel is only interacting with element-size fragments. For traction operation, all fragments are fed into the wheel-rail interface with the help of the rolling wheel and the deformable rail (Fig. 4(c)). However, in braking case, the majority of fragments have been held and pushed away by the sliding wheel till the end of the simulation and limited fragments are able to pass through the wheel-rail contact (Fig. 4(f)).

3.2. Particle size analysis

During traction operation, the results of adhesion enhancement for particle sizes from 0.71 mm to 2 mm are given in Fig. 5(a). The adhesion enhancement calculated at the fracture stage is negligible for all particles compared with the values from the post-fracture stage. The adhesion enhancement starts to increase sharply due to the wheel rolling on fragments. When all fragments break into element sizes, the adhesion enhancement achieves its peak value and then begins to decline as the wheel is passing the enhanced area. The variation trend of adhesion enhancement observed from different particles is similar, but the magnitude grows when particle size increases.

Since the element size of 0.1 mm was assigned to all the particle meshes, the number of element size fragments generated during the fracture stage varies from mesh to mesh. Therefore, the generated

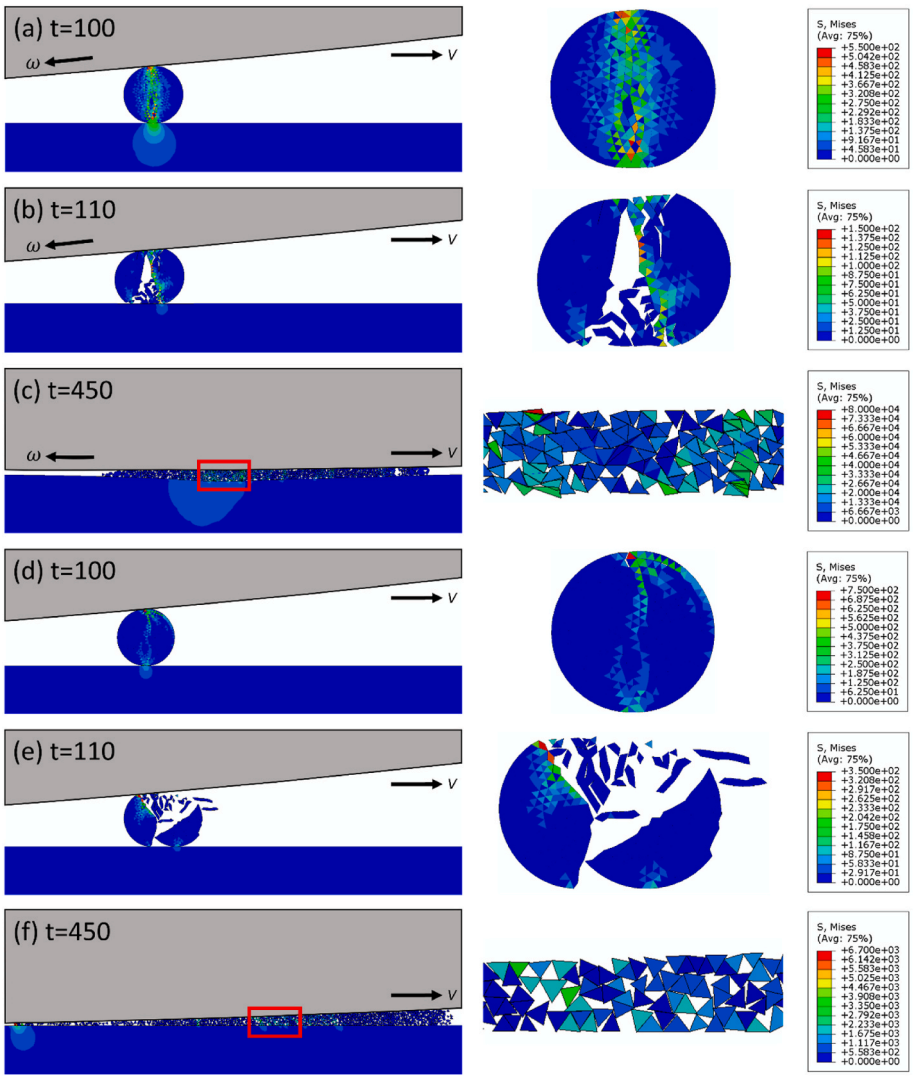

Fig. 4. Fracture process of single particle. (a)–(c) traction operation and (d)–(f) braking operation.

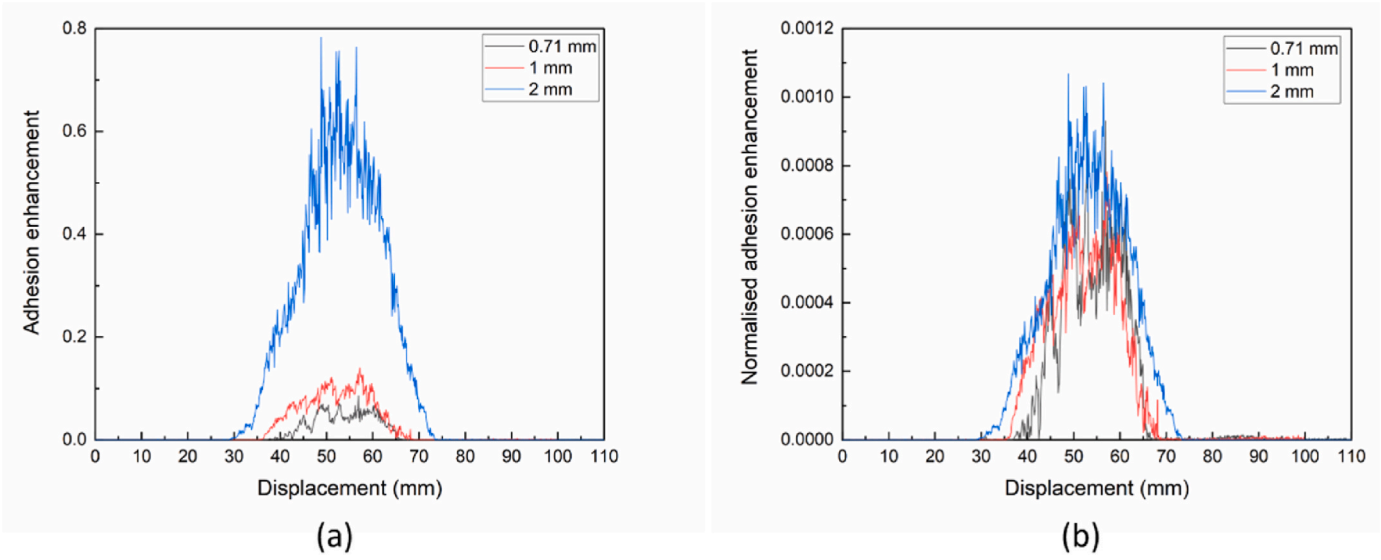

Fig. 5. Size effect during traction operation. (a) adhesion enhancement of single particle and (b) normalized adhesion enhancement.

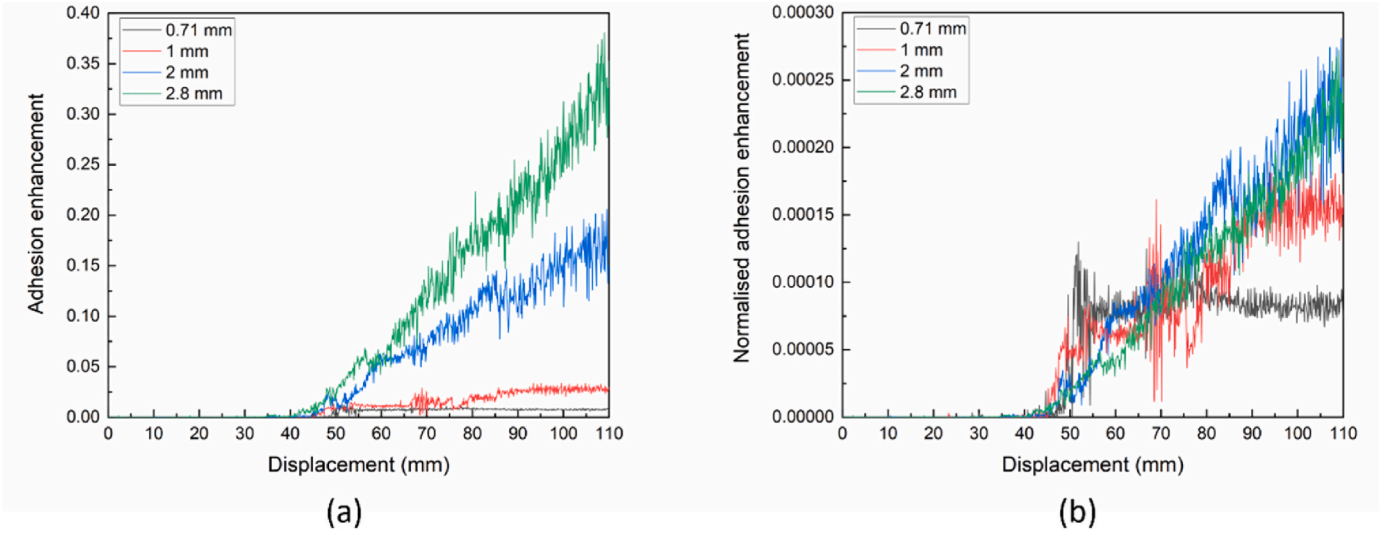

Fig. 6. Size effect during braking operation. (a) adhesion enhancement of single particle and (b) normalized adhesion enhancement.

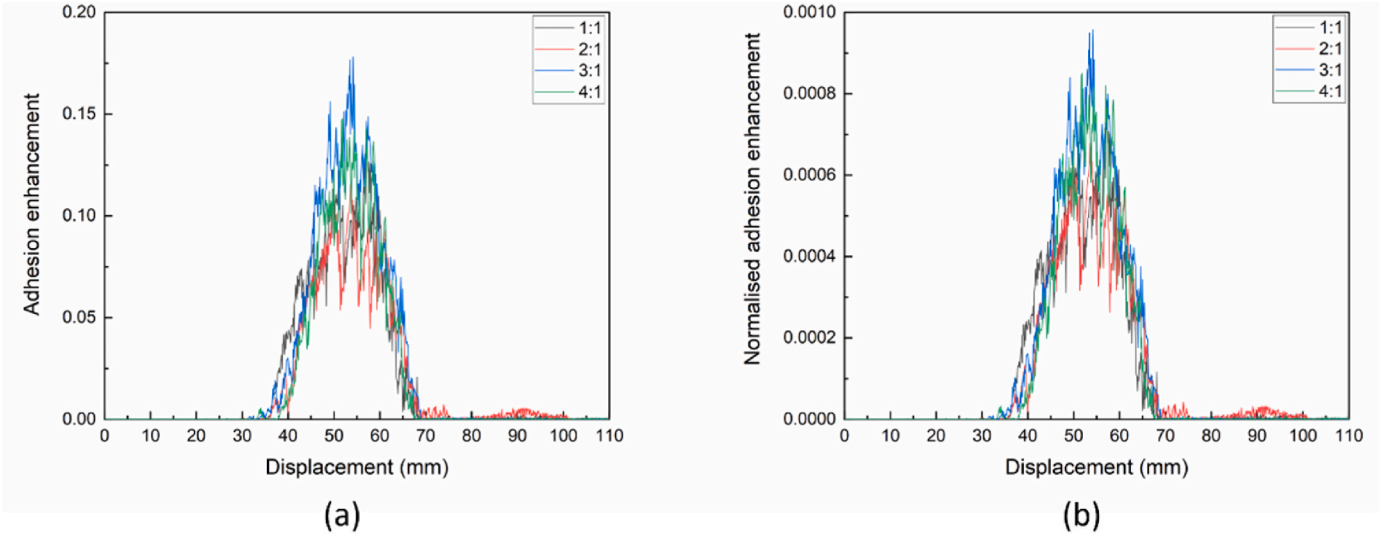

Fig. 7. Shape effect during traction operation. (a) adhesion enhancement of a single particle and (b) normalized adhesion enhancement.

adhesion enhancement has been divided by the total number of fragments for each case and the results have been plotted in Fig. 5(b) to investigate the contribution of fragment number to the adhesion. After the normalization, the variation trends are similar to the non-normalized ones, but the magnitude is now converging. This can be related to the mass of fragments considering the fact that they are assumed to be homogenous with constant density. In more scientific terms, the new surface area generated as the third body in the contact is similar after the normalization.

For braking operation, particle sizes ranging from 0.71 mm to 2.8 mm are used and the results are plotted in Fig. 6. A clear increase for all particles is observed at a bigger displacement owing to chopping fragmentation as fragments further spread along the rail. Due to the different amount of fragments generated, the increment slope is steep for bigger particles and is gentle for smaller particles, as shown in Fig. 6(a). The smaller particles (i.e., 0.71 mm and 1 mm) achieved a lower plateau quickly. The bigger particles (i.e., 2 mm and 2.8 mm), on the other hand, keep increasing till the end due to the simulation length. This indicates that it takes a larger displacement for big amount of fragments to achieve a plateau. Normalization is conducted to the data and the results are indicated in Fig. 6(b). All the increasing trends are overlapping now. The peak value for a single fragment (ca. 0.00025) is smaller than the one (ca. 0.0010) in the traction operation (Fig. 5(b)).

The results before and after normalization reveal the fact that the adhesion enhancement is induced by the fragments generated, not the particle size. Additionally, sand particles during traction operation tend to provide a higher adhesion enhancement than the braking operation. On the other hand, the improvement lasts longer during braking operation owing to the fragments carryover event.

3.3. Particle shape analysis

The particle shape is another important morphological parameter affecting mechanical behaviour. Therefore, a set of ellipsoidal meshes with a different aspect ratio ranging from 1:1 to 4:1 are used to study the shape effect on adhesion enhancement. As it was revealed in particle size analysis that different amounts of fragments could lead to different traction enhancement results, certain dimensions were selected to generate meshes to not only meet the different aspect ratios, but also to consist of a similar amount of fragment elements.

During traction operation, four different particle meshes were tested and the results of adhesion enhancement are shown in Fig. 7(a). Overall,

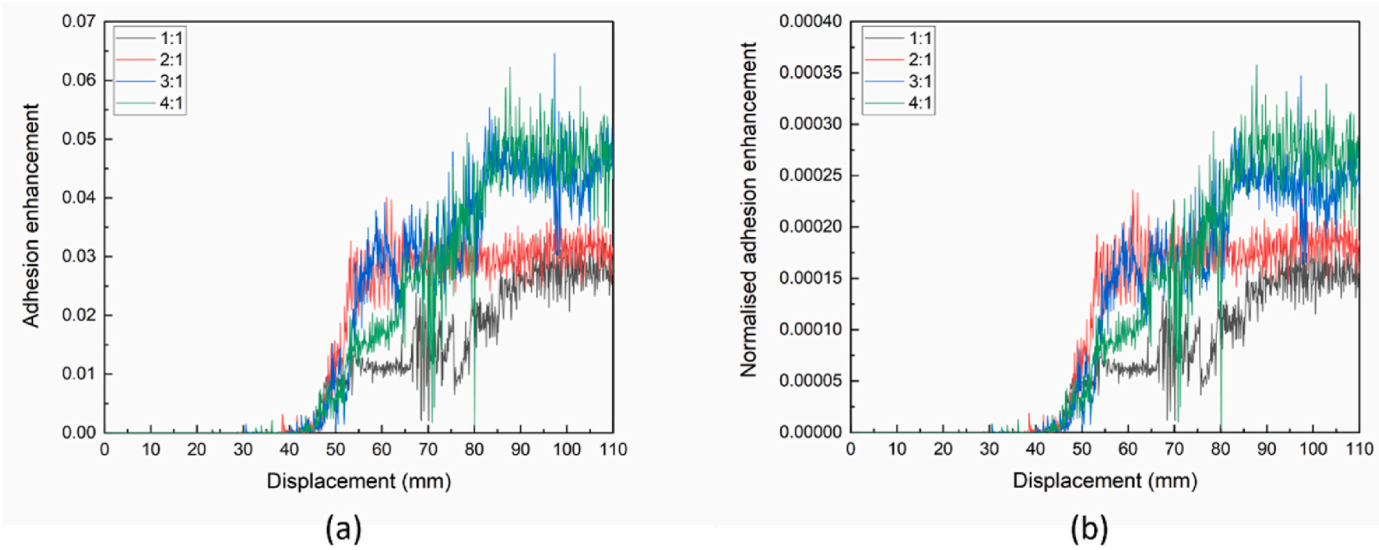

Fig. 8. Shape effect during braking operation. (a) adhesion enhancement of single particle and (b) normalized adhesion enhancement.

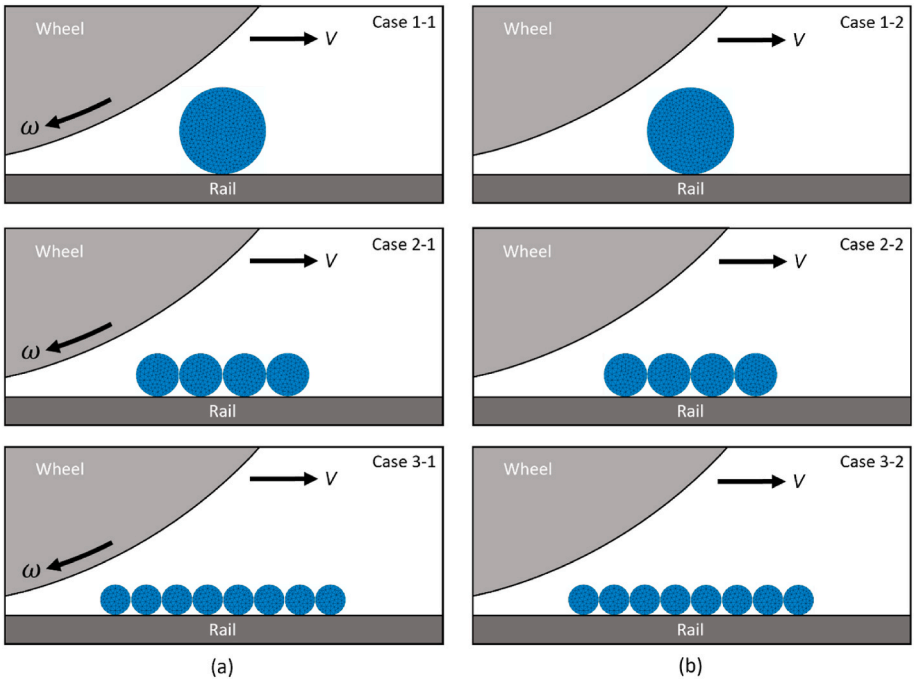

Fig. 9. Particle combinations during (a) traction operation and (b) braking operation.

the plot of adhesion enhancement from different particle meshes shows the same variation trend with a similar peak value. This indicates that changing aspect ratio is not affecting the adhesion enhancement significantly. Fig. 7(b) illustrates the results after normalization. As fragments generated from different particle meshes are comparable, the plots are similar to the non-normalized ones, however, the values are now for the single fragment. These values are identical to the normalized data in particle size analysis.

For braking operation, the same particle meshes are used and the results of adhesion enhancement are given in Fig. 8(a). Overall, all plots of adhesion enhancement start to increase at the same location with a similar slope. However, the plots of particle mesh with a smaller aspect ratio (i.e., 1:1 and 2:1) reach a lower peak value earlier and maintain it till the end of the simulation. On the other hand, the plots of particle mesh with a larger aspect ratio (i.e., 3:1 and 4:1) achieve a higher peak value at a later stage. This is owing to the fragments of elongated shape spreading widely along the rail after breakage and thus generating a larger fragment-to-wheel contact area. After the normalization, the plots are identical to the non-normalized ones due to the similar amount of fragments, however, the separation between each plateau becomes more obvious that the single fragment from the elongated shape tends to provide a higher adhesion enhancement.

Similar results are observed in particle shape analysis that the adhesion enhancement during traction operation is higher than the braking operation. Moreover, during the braking operation, the elongated shape is able to generate a higher adhesion enhancement compared to the circular shape.

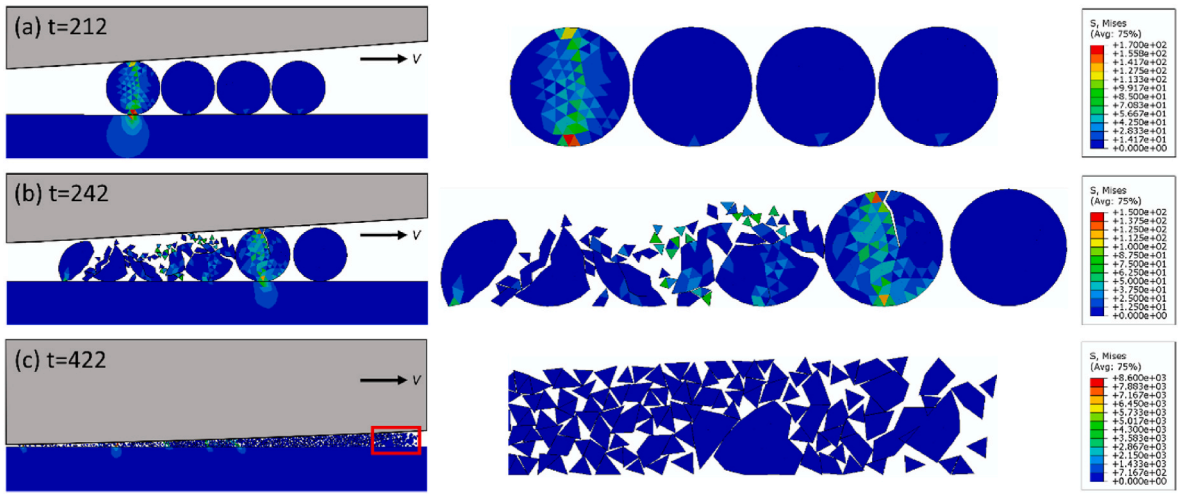

Fig. 10. Fracture process of Case 2-2.

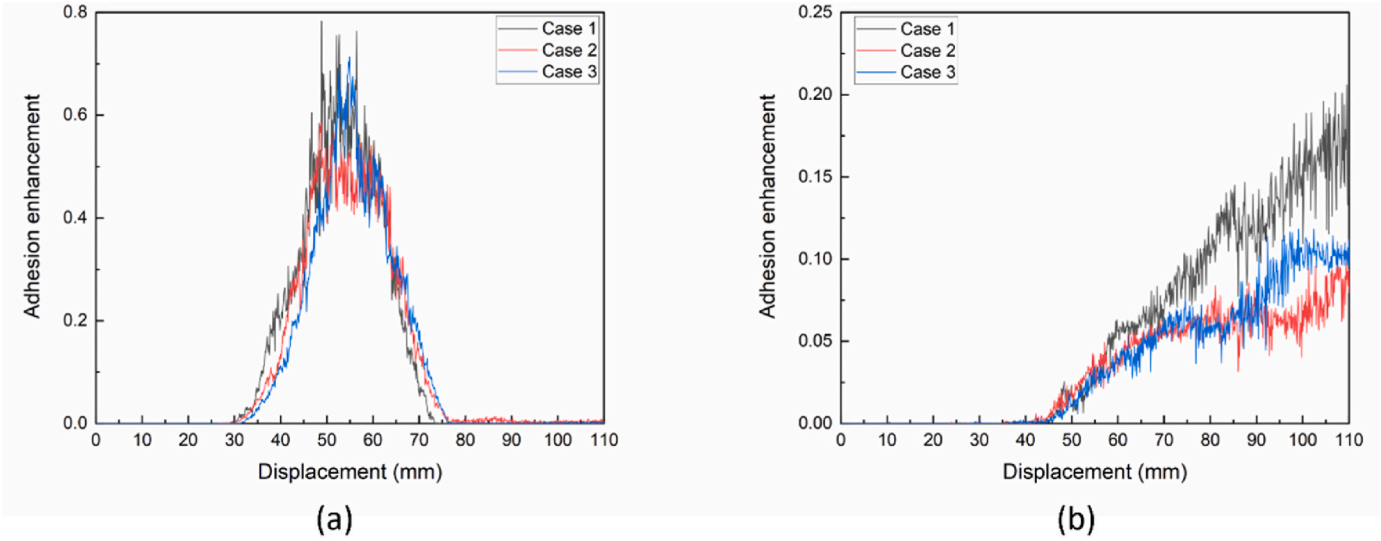

Fig. 11. Number effect on adhesion enhancement during (a) traction operation and (b) braking operation.

3.4. Multi-particles analysis

In addition to the size and shape analysis, the effect of particle number on adhesion enhancement is investigated. Similarly, in order to minimize the influence of fragment number on the adhesion enhancement, different combinations of particles, consisting of a similar amount of CPE3 elements, are used. Thus, a 2 mm circular mesh with 733 elements, four 1 mm circular meshes with a total amount of 716 elements, and eight 0.71 mm circular meshes with a total amount of 736 elements have been adopted in Cases 1, 2 and 3, respectively, as shown in Fig. 9. Additionally, the fracture process of Case 2-2 has been illustrated in Fig. 10 to demonstrate the breakage behaviour of multi-particles.

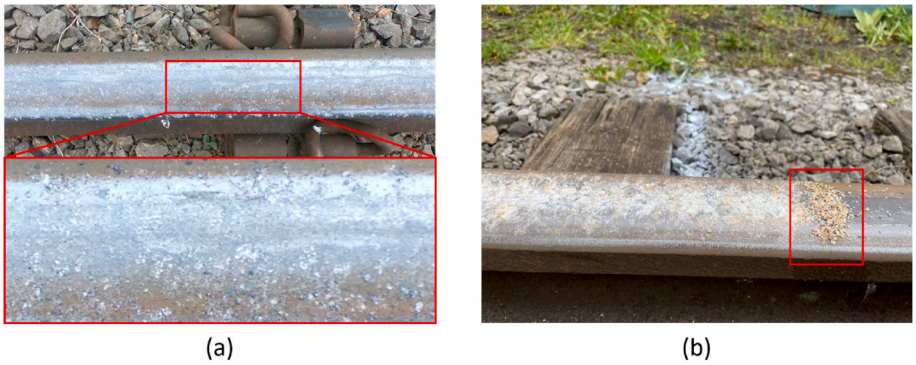

Fig. 12. Sand fragments on the rail during (a) traction operation and (b) braking operation.

The results of adhesion enhancement for three cases during traction operation are given in Fig. 11(a). Although the particle numbers are different from case to case, the plots of adhesion enhancement coincide with each other, as the total amount of fragments generated during the fracture event is similar for different cases. However, the results from the braking operation provide a different relationship as shown in Fig. 11(b). With a similar increasing slope, the case with a single particle ends with a higher adhesion enhancement. This is due to the fracture behaviour of multi-particles. As particles were breaking one by one, with more obvious sliding movement to the later particles (Fig. 10(b) and (c)). This fracture behaviour results in a constant feeding of the particle-size amount of fragments to the wheel-rail contact, which is considerably lower than the one bigger particle consisting of the full amount of fragments.

Considering the results from particle size, shape and number analysis, the traction operation is a fragment-based process. The adhesion enhancement is mainly influenced by the number of fragments at the wheel-rail contact. On the contrary, adhesion enhancement during the braking operation considers all the effects of particle size, shape and number simultaneously. Based on these simulations, larger size particle with an elongated shape is preferred for the braking operation.

During our recent test track experiments, the sand fragments on the rail have been observed after each operation. Fragments were passed over by the wheel and left on rail during traction operation as shown in Fig. 12(a) and have been pushed to the end of braking operation as shown in Fig. 12(b). These experimental observations demonstrate a good agreement with the simulation results. It is recommended to record the traction force and normal force from the wheel during a sanding process to establish a link between the field test and the mentioned simulation method.

4. Conclusions

In this study, a FEM approach coupled with CIEs has been adapted to investigate the adhesion improvement at the wheel-rail interface due to sand particle breakage. The fracture behaviour of particles during traction and braking operation has been analysed. The effect of particle size, shape and number on the adhesion enhancement has been compared. The main conclusions withdrawn from this study are as follows:

- Adhesion enhancement triggered by sand particles can be correlated to the number of generated fragments, in other words, adhesion improvement is caused by the newly generated surface area of the third body.
- Sand particles provide a higher adhesion enhancement during the traction operation compared to the braking operation.
- During traction operation, the adhesion enhancement is influenced by the number of fragments, regardless of the particle size, shape and number.
- During braking operation, for particles with a similar total amount of fragments, the coarser and more elongated particle generates a higher adhesion enhancement.

The methodology in this study provides a framework for exploring the adhesion enhancement induced by particle fragments. A future work considering a mix of particle sizes and shapes will be conducted to reproduce real cases by utilizing an in-house code to insert CIEs into 3D meshes; extra efforts will be given in the simulation of particle breakage in a 3D environment and its possible influence on adhesion.

Declaration of competing interest

The authors declare that they have no known competing financial interests or personal relationships that could have appeared to influence the work reported in this paper.

Data availability

Data will be made available on request.

Acknowledgements

The first author is funded by China Scholarship Council – Newcastle University Scholarships (CSC-NU). The authors acknowledge the support of the UK Engineering and Physical Sciences Research Council (EPSRC) grant No. EP/V053655/1 RAILSANDING - Modelling Particle Behaviour in the Wheel-Rail Interface.

References

[1] William A. Skipper, Anup Chalisey, Roger Lewis, A review of railway sanding system research: adhesion restoration and leaf layer removal, Tribol. Mater. Surface Interfac. 12 (4) (2018) 237–251, https://doi.org/10.1080/17515831.2018.1542791.
[2] C.R. Fulford, Review of Low Adhesion Research, Rail Safety and Standards Board, UK, 2004. Report published by the.
[3] Rail Accident Report, Autumn adhesion investigation Part 3 review of adhesion-related incidents, Rail Accident Investigation Branch, Department for Transport, 2007. URL: https://assets.publishing.service.gov.uk/media/547c906840f0b602440001ad/R252006_070108_Part_3_Adhesion_Review.pdf.
[4] Kei Ishizaka, Stephen R. Lewis, Roger Lewis, The low adhesion problem due to leaf contamination in the wheel/rail contact: bonding and low adhesion mechanisms, Wear 378 (2017) 183–197, https://doi.org/10.1016/j.wear.2017.02.044.
[5] T.M. Beagley, C. Pritchard, Wheel/rail adhesion—the overriding influence of water, Wear 35 (2) (1975) 299–313, https://doi.org/10.1016/0043-1648(75)90078-2.
[6] T.M. Beagley, I.J. McEwen, C. Pritchard, Wheel/rail adhesion—boundary lubrication by oily fluids, Wear 31 (1) (1975) 77–88, https://doi.org/10.1016/0043-1648(75)90123-4.
[7] Yi Zhu, The influence of iron oxides on wheel–rail contact: a literature review, Proc. Inst. Mech. Eng. F J. Rail Rapid Transit 232 (3) (2018) 734–743, https://doi.org/10.1177/0954409716689187.
[8] S.R. Lewis, S. Riley, D.I. Fletcher, R. Lewis, Optimisation of a railway sanding system for optimal grain entrainment into the wheel–rail contact, Proc. Inst. Mech. Eng. F J. Rail Rapid Transit 232 (1) (2018) 43–62, https://doi.org/10.1177/0954409716656220.
[9] Aishwarya Gautam, Sheldon I. Green, Computational fluid dynamics–discrete element method simulation of locomotive sanders, Proc. Inst. Mech. Eng. F J. Rail Rapid Transit 235 (1) (2021) 12–21, https://doi.org/10.1177/0954409720902897.
[10] W. Skipper, S. Nadimi, R. Lewis, Sand Consist Changes for Improved Track Circuit Performance (COF-UOS-03), 2021. https://www.rssb.co.uk/en/research-catalogue/CatalogueItem/COF-UOS-03.
[11] Rail Safety and Standards Board, GMRT2461 Sanding Equipment (Issue 3), 2018, pp. 1–24.
[12] P.R. Cooper, An Investigation into the Relationship between the Particle Size and the Frictional Performance of Sand (IM-ADH-011), British Rail Report), 1972.
[13] W.A. Skipper, S. Nadimi, A. Chalisey, R. Lewis, Particle characterisation of rail sands for understanding tribological behaviour, Wear 432 (2019) 202960, https://doi.org/10.1016/j.wear.2019.202960.
[14] O. Arias-Cuevas, Z. Li, R. Lewis, Investigating the lubricity and electrical insulation caused by sanding in dry wheel–rail contacts, Tribol. Lett. 37 (2010) 623–635, https://doi.org/10.1007/s11249-009-9560-1.
[15] L.B. Shi, C. Wang, H.H. Ding, D. Kvarda, R. Galas, M. Omasta, W.J. Wang, Q.Y. Liu, M. Hartl, Laboratory investigation on the particle-size effects in railway sanding: comparisons between standard sand and its micro fragments, Tribol. Int. 146 (2020) 106259, https://doi.org/10.1016/j.triboint.2020.106259.
[16] W.A. Skipper, S. Nadimi, M. Watson, A. Chalisey, R. Lewis, Quantifying the effect of particle characteristics on wheel/rail adhesion & damage through high pressure torsion testing, Tribol. Int. 179 (2023) 108190, https://doi.org/10.1016/j.triboint.2022.108190.
[17] Oscar Arias-Cuevas, Zili Li, Roger Lewis, A laboratory investigation on the influence of the particle size and slip during sanding on the adhesion and wear in the wheel–rail contact, Wear 271 (1–2) (2011) 14–24, https://doi.org/10.1016/j.wear.2010.10.050.
[18] Xin Zhao, Zili Li, The solution of frictional wheel–rail rolling contact with a 3D transient finite element model: validation and error analysis, Wear 271 (1–2) (2011) 444–452, https://doi.org/10.1016/j.wear.2010.10.007.
[19] Keyvan Zare-Rami, Yong-Rak Kim, MIDAS-VT-Pre: software to generate 2D finite element model of particle/fiber embedded composites with cohesive zones, SoftwareX 10 (2019) 100292, https://doi.org/10.1016/j.softx.2019.100292.
[20] M.L. Benzeggagh, M.J.C.S. Kenane, Measurement of mixed-mode delamination fracture toughness of unidirectional glass/epoxy composites with mixed-mode

bending apparatus, Compos. Sci. Technol. 56 (4) (1996) 439–449, https://doi.org/10.1016/0266-3538(96)00005-X.

[21] Zoheir Aboura, Etude du processus de délaminage mode I, mode II et mode mixte (I + II) de matériaux composites à renforts tissés à différentes vitesses de sollicitation, PhD diss, Compiègne, 1993.

[22] Bin Zhang, Sadegh Nadimi, Eissa Ali, Rouainia Mohamed, Modelling fracturing process using cohesive interface elements: theoretical verification and experimental validation, Construct. Build. Mater. 365 (2023) 130132, https://doi.org/10.1016/j.conbuildmat.2022.130132.